ANL/CMT/CP-103107

CORROSION OF STRUCTURAL MATERIALS BY LEAD-BASED REACTOR COOLANTS[1]

by

D. P. Abraham, L. Leibowitz, V. A. Maroni, S. M. McDeavitt, and A. G. Raraz

Argonne National Laboratory
Chemical Technology Division
9700 S. Cass Ave.
Argonne, IL 60439

Phone: (630) 252-4332
Fax: (630) 252-9917
e-mail: abraham@cmt.anl.gov

To be presented at the International Atomic Energy Agency
November 28-December 1, 2000
Argonne National Laboratory

[1]Work supported by the U.S. Department of Energy, Nuclear Energy Research & Development Program, under Contract W-31-109-Eng-38

DISCLAIMER

CORROSION OF STRUCTURAL MATERIALS BY LEAD-BASED REACTOR COOLANTS

D. P. Abraham, L. Leibowitz, V. A. Maroni, S. M. McDeavitt, and A. G. Raraz

Abstract

Advanced nuclear reactor design has, in recent years, focused increasingly on the use of heavy-liquid-metal coolants, such as lead and lead-bismuth eutectic. Similarly, programs on accelerator-based transmutation systems have also considered the use of such coolants. Russian experience with heavy-metal coolants for nuclear reactors has lent credence to the validity of this approach. Of significant concern is the compatibility of structural materials with these coolants. We have used a thermal convection-based test method to allow exposure of candidate materials to molten lead and lead-bismuth flowing under a temperature gradient. The gradient was deemed essential in evaluating the behavior of the test materials in that should preferential dissolution of components of the test material occur we would expect dissolution in the hotter regions and deposition in the colder regions, thus promoting material transport. Results from the interactions of a Si-rich mild steel alloy, AISI S5, and a ferritic-martensitic stainless steel, HT-9, with the molten lead-bismuth are presented.

Introduction

Advanced nuclear reactor design has, in recent years, focused increasingly on the use of heavy-metal coolants, such as lead and lead-bismuth eutectic [1]. Similarly, programs on accelerator-based transmutation systems [2] have also considered the use of such coolants. Russian experience with heavy-metal coolants for nuclear reactors has lent credence to the validity of this approach [3]. The advantages and disadvantages of such coolants has been previously reviewed [4] and will not be discussed here.

Interest in the use of lead and lead alloys as coolants in nuclear reactors has a long history going back to the 1950s. In the United States, however, sodium became the coolant of choice in fast reactors because of some superior properties. An extensive development program was undertaken on sodium cooling and work on lead-cooled reactors was given considerably less attention. In contrast, researchers in the Soviet Union continued work on lead-based coolants and according to their reports had considerable success. In spite of the earlier choice of sodium there are significant advantages to the use of lead and lead-based alloys. Substituting lead for sodium eliminates a significant combustion hazard. In addition, the high boiling point of lead allows for potentially much higher operating temperatures. Prominent among the disadvantages of using lead as a reactor coolant are uncertainties regarding corrosion and liquid-metal embrittlement.

The compatibility of structural materials with lead-based coolants is of pivotal concern in nuclear reactor technology and several studies have been reported in the literature. Early work at Argonne National Laboratory [5] reported in 1955 (actually performed in 1949) involved static immersion tests of the compatibility of a number of materials with molten lead at 1000^0C. Sintered beryllia, fused silica, tantalum, and niobium were reported to have good resistance to

lead. However, the results of static tests can be misleading because they do not account for material transport under a temperature gradient. Thermal convection loops were constructed and operated at Brookhaven National Laboratory [6] with the hot leg at roughly 500^0C and the cold leg at about 400^0C. Relatively low liquid velocities, averaging around 0.05 ft/sec were obtained, but more importantly, the potential for material transport existed. Material testing in thermal convection loops has also been reported by researchers in Russia [3], the United Kingdom [7] and Germany [8].

This article presents corrosion results for alloys exposed to molten lead-bismuth flowing under a temperature gradient. The gradient was deemed essential in evaluating alloy behavior because it allowed for the possibility of material transport. Preferential dissolution was expected in the hotter regions of the test assembly and material deposition was expected in the colder regions. A test system used successfully by researchers at Oak Ridge National Laboratory [9] was adapted for our experiments. Iron-based alloys containing alloying elements expected to form stable protective oxides were selected for testing. These were AISI S-5, a 2 wt% Si mild steel and HT-9, a Cr-bearing ferritic-martensitic stainless steel, chosen because it approximates the composition of a Russian steel, EP-823, claimed to be very resistant to lead corrosion. Nominal alloy compositions are shown in Table 1. A comparison of alloy corrosion characteristics demonstrates the crucial role of chromium in the passivation behavior of iron-based alloys.

Experimental

A schematic of the quartz convection harp installed in a furnace assembly is shown in Fig. 1. Tubular samples of AISI S-5 (test H-2) and X-shaped samples of HT-9 were fabricated from available stock. Test samples were placed in the center of the two vertical legs of the harp and held in place with dimples above and below the samples. The quantity of granular Pb-Bi eutectic needed to fill the harp was placed in the large bulb (see Fig. 1) for treatment prior to introduction into the harp. A porous quartz frit below the bulb prevented the metal from running into the harp prematurely. The harp-furnace enclosure assembly was mounted in a ventilated hood containing a specially designed gas-handling system. The harp was evacuated and flushed several times with He-4% H_2 (He-H_2) sweep gas then heated to ~350°C with sweep gas flowing through it. Heating tape was wrapped around the large bulb and the Pb-Bi eutectic was melted. Sweep gas was allowed to bubble through the molten Pb-Bi and the moisture content of the exit gas was measure using a Panametrics Series 3 moisture monitor. When the moisture level reached ~25 ppm the arm below the frit (see Fig. 1) was evacuated and pressure (He-H_2) was applied above the molten eutectic, forcing the liquid metal into the harp. Sweep gas was continually passed over the molten Pb-Bi for the entire duration of the experiment.

Temperature controllers were provided on the two vertical legs and Variacs supplied power, as needed to the upper and lower slanted branches of the harp. Following filling, the hot leg temperature was raised to 550°C. Temperatures were monitored using a National Instruments data logger. The cold leg controller was set at 350°C; however, heat transport from the hot leg was sufficient to raise the cold-leg temperature above the cold leg set point by about 50-75°C. Attempts were made to determine the flow rate of the eutectic by introducing a brief cold pulse of air to the top branch of the harp and observing the appearance of a brief thermal dip on the

cold leg. From the signals obtained we were able to estimate a flow rate of ~ 30.5 cm/min (1 ft/min), similar to that reported in [9].

The harp systems operated with excellent thermal and flow stability for 4500 hours, after which they were shut down for examination. Each harp was disassembled and the sections containing the test pieces were placed in separate filtering tubes, shown in Fig. 2, to remove as much adhering Pb-Bi as possible. These filtering tubes operated like the harp filling system. Heating tape was wrapped around the upper section to melt the eutectic. Evacuation and pressurization, conducted as for the fill operation, forced the molten metal into the lower chamber leaving the test alloy with a thin coating of Pb-Bi in the upper section. In separate procedures, a sample of Pb-Bi was treated with He-H_2 and filtered to provide a control sample that was not exposed to the alloys tested.

Samples of lead-bismuth from the control, and from the harp containing the HT-9 specimens were analyzed by ICP/AES. The HT-9 was examined using Raman spectroscopy, Auger electron spectroscopy (AES), scanning electron microscopy (SEM), transmission electron microscopy (TEM), and X-ray diffraction (XRD). The AISI S-5 sample has, to date, been examined only by SEM. Results of these examinations are given below.

Results

Examination of the AISI S-5 samples

Visual examination of the test samples showed a black discoloration under the adhering lead-bismuth alloy. Sections of the exposed samples were examined by scanning electron microscopy (SEM). Micrographs from a sample in the hot leg (~550°C) are shown in Figs. 3a and 3b. Intergranular penetration of lead-bismuth into the sample is plainly evident in Fig. 3a, making this material a poor candidate for structural applications. The depth of penetration ranged from 10 μm to 40 μm. A non-adherent scale, rich in Si, Fe and O, was found on the sample surface; the nature of this scale is being determined by X-ray diffraction. This scale is evident in Fig. 3b, which clearly shows the debris left behind after the sample was attacked. Samples from the cold leg (~350-425°C) also showed some attack. However, the depth of penetration in these samples ranged from 1-5 μm. The difference in attack in the hot and cold legs clearly demonstrates the influence of temperature on alloy corrosion.

Examination of the HT-9 samples

The appearance of harp H-1 (containing the HT-9 samples) after test termination is shown in Fig. 4. Note that the quartz cracked on cooling. The lead-bismuth, however, was quite shiny and showed no obvious signs of contamination. The elemental analyses of the Pb-Bi samples are shown in Table 2. Although some of the changes appear to be outside the reported analytical uncertainty, no major differences are seen between the exposed samples and the control sample. However, decreases in Fe and Ni and increases in Cu and Sn in the exposed Pb-Bi samples are noteworthy. Visual observation of the HT-9 samples revealed a black coating under an adherent lead-bismuth layer (see Fig. 5). This black coating was not present on the original HT-9. Considerable effort was devoted to the characterization of this layer.

Samples from both the hot and cold legs were examined by SEM. The studies showed that the Pb-Bi did not penetrate the samples. A thin surface layer (see Fig. 6), ranging from 0.1 to 0.2 μm was observed on samples in the hot leg (~550°C). Detailed SEM-EDS analysis could not be conducted because the surface layer was too thin. However, cursory analysis indicated that the layer was enriched in chromium. Examination of samples in the cold leg revealed no obvious surface film; any layer present was apparently too thin to be seen under the SEM.

The corrosion product on one hot leg sample was examined by Auger Electron Spectroscopy (AES). The samples were sputtered with argon (Ar^+) ions to measure elemental composition as a function of depth. A ~10 nm lead-bismuth layer present on the top surface was initially removed by sputtering. A typical AES depth profile is shown in Fig. 7; other areas examined on the sample showed essentially the same result. Only Fe, Cr and O were observed in the corrosion layer. Furthermore, the data clearly showed chromium-enrichment in areas near the oxide-molten metal interface.

Raman spectra of the surface of a hot leg sample were recorded using a Renishaw System 2000 Imaging Raman Microscope. The spectra were obtained with the specimen surface perpendicular to the excitation/observation directions. The spectra obtained were similar to those observed previously for mildly oxidized iron-chromium alloys [10]. The oxide film was identified as being of the $Fe_{3-x}Cr_xO_4$-type. From the specific band shape and peak frequencies we inferred that x was substantially greater than zero, i.e., the oxide film was rich in chromium.

Low angle X-ray diffraction (XRD) patterns were obtained on the samples at the Advanced Photon Source (APS) at Argonne National Laboratory (ANL). A sample with the black layer exposed was mounted in a diffractometer at the MRCAT beam line. Diffraction patterns were obtained with the sample at a constant angle of 3.5° or 6.5° to the beam. A conventional θ-2θ scan, in which the beam penetration varies with incident angle, was also obtained with a beam energy of 11 keV (wavelength=0.11271 nm). Analysis of the diffraction peaks indicated the existence of a $FeCr_2O_4$-type spinel on the sample.

Preliminary transmission electron microscopy (TEM) results have confirmed the existence of an adherent $FeCr_2O_4$-type spinel on the sample surface. The analysis has shown that the spinel layer is ~100-150 nm (0.1-0.15 μm thick). Crystalline particles with $BiPb_3$- or $BiPb_4$-type structure containing Fe and Cr have also been observed on the sample surface. The TEM observations are consistent with the results of XRD, Raman spectroscopy and AES.

Discussion

The formation of an oxide film on an alloy surface is determined by temperature, oxide stability and oxygen activity in the system. The relationships involved can be illustrated for the case of Cr_2O_3. For one mole of oxygen, the relevant equation for Cr_2O_3 formation is:

$$4/3\ Cr + O_2 = 2/3\ Cr_2O_3 \qquad (1)$$

The equilibrium constant for this reaction is

$$K = (a_{Cr2O3})^{2/3} / (a_{Cr})^{4/3}\ P_{O2}$$

Where, a_{Cr} and a_{Cr2O3} are the activities of Cr and Cr_2O_3, respectively and P_{O2} is the oxygen pressure. If the activities of the solids are assumed to be unity, then the oxygen pressure is the reciprocal of the equilibrium constant.

At 550°C the Gibbs energy change for reaction (1) is -146.7 kcal yielding an equilibrium constant of 9.06×10^{38} and the equilibrium oxygen pressure will be $\sim 10^{-39}$ atm. Thus at 550°C, Cr_2O_3 will only form at pressures higher than $\sim 10^{-39}$ atm. Similar calculations can be carried out for other oxides by using reference data available in literature. Table 3 summarizes the equilibrium oxygen pressures for various oxides assuming condensed phases at unit activity.

The oxygen partial pressure in our system can be roughly estimated from the measured moisture content (about 10 ppm) and the hydrogen concentration in the He-H_2 cover gas (about 4 %). From the known Gibbs energy of formation of water we estimate P_{O2} in our system at 550°C to be about 1×10^{-33}, much larger than needed to form Cr_2O_3 or $FeCr_2O_4$, but very much lower than that needed to form PbO. Clearly the existing oxygen partial pressure in our system permits formation of the Cr-containing oxides but not PbO or Bi_2O_3. Table 3 shows that the oxygen partial pressure for formation of Cr_2O_3 and the spinel $FeCr_2O_4$ are very close. The spinel structure may be favored on HT-9 because of the high iron content of the samples.

Summary and Conclusions

An experimental setup was designed and used to test iron-based alloys alloys exposed to molten lead-bismuth flowing under a temperature gradient. The temperature in the hot leg of the convection harp was ~550°C and the temperature in the cold leg was ~350-425°C. The alloys chosen for the test were AISI S-5, a 2 wt% Si mild steel, and HT-9, a ferritic-martensitic stainless steel. The tests were terminated after sample exposure for ~4500 hours. The results of our studies may be summarized as follows:

1. The AISI S-5 alloy was attacked by the molten lead-bismuth. The depth of intergranular penetration ranged up to 40 μm in the hot leg and up to 5 μm in the cold leg. The test showed that AISI S-5 would not be suitable as a structural material for nuclear reactors using lead-based alloy coolants.
2. The HT-9 samples were not attacked by the molten lead-bismuth. The samples appear to have been protected by a stable, adherent, $FeCr_2O_4$-type spinel layer. Close control of oxygen activity was not necessary to form the protective spinel. As long as the oxygen activity is well below that needed to form PbO and above that needed to form the spinel, ample leeway exists to form a protective layer on HT-9.
3. A comparison of AISI S-5 and HT-9 corrosion behavior clearly demonstrates the important role of chromium in the passivation of HT-9 and EP-823 alloys exposed to molten Pb-Bi.

Acknowledgements

The authors gratefully acknowledge the assistance of D. E. Preuss for design, G. L. Chapman for electronics, C. C. McPheeters for conceptual support, A. J. Kropf for x-ray diffraction measurements, N. Finnegan for AES measurements and Dean J. Miller and Zhiping Luo for the TEM study.

References

1. B. W. Spencer, R. N. Hill, D. C. Wade, D. J. Hill, J. J. Sienicki, H. S. Khalil, J. E. Cahalan, M. T. Farmer, V. A. Maroni, and L. Leibowitz, " An Advanced Modular HLMC Reactor Concept Featuring Economy, Safety, and Proliferation Resistance", Proceedings of the 8th International Conference on Nuclear Engineering, Baltimore, MD, 2000.

2. J. J. Park and J. J. Buksa, "Selection of Flowing Lead Target Structural Materials for Accelerator Driven Transmutation Applications", Proc. International Conference on Accelerator-Driven Transmutation Technologies and Applications, Las Vegas, NV, 1994.

3. B. F. Gromov, Yu. I. Orlov, P. N. Martynov, K. D. Ivanov, and V. A. Gulevsky, "Physical-Chemical Principles of Lead-Bismuth Coolant Technology", pp. 339-343 in "Liquid Metal Systems" H. U. Borgstedt Ed, Plenum, New York, 1995.

4. for example see B. W. Spencer "The Rush to Heavy Liquid Metal Reactor Coolants - Gimmick or Reasoned" Proceedings of the 8th International Conference on Nuclear Engineering, Baltimore, MD, 2000.

5. W. D. Wilkinson, E. W. Hoyt, and H. V. Rhude, "Attack on materials by lead at 1000^0C", Argonne National Laboratory Report, ANL-5449, 1955.

6. A. J. Romano, C. J. Klamut, and D. H. Gurinsky, "The investigation of container materials for Bi and Pb alloys, Part I, Thermal convection loops." Brookhaven National Laboratory Report, BNL 811 (T-313), 1963.

7. R. C. Asher, D. Davies, and S. A. Beetham, "Some observations on the compatibility of structural materials with molten lead", Corr. Sci., 17, (1977) pp. 545-557.

8. G. Muller, G. Schumacher, and F. Zimmermann, J. Nucl. Mater., 278 (2000) pp. 85-95.

9. J. V. Cathcart and W. D. Manley, "A Technique for Corrosion Testing in Liquid Lead", Corrosion 10 432 (1954).

10. V. A. Maroni, C. A. Melendres, T. F. Kassner, R. Kumar, and S. Siegel, "Spectroscopic Characterization of Oxide Films on Type 304 SS Exposed to Water at 289°C: Correlation with the Fe-Cr-H_2O Pourbaix Diagram", J. Nucl. Mater., 172, 13 (1990).

11. R. A. Robie, B. S. Hemingway, and J. R. Fisher, "Thermodynamic Properties of Minerals and Related Substances at 298.15 K and 1 Bar (10^5 Pascals) Pressure and at Higher Temperatures", Geological Survey Bulletin 1452, United States Government Printing Office, Washington, 1978.

12. I. Barin, "Thermochemcial Data of Pure substances", Third Ed., VCH Publishers, New York, 1995.

List of Tables

List of Figures

Table 1. Composition (wt%) of HT-9, AISI S-5, and EP-823

	Ni	Cr	Mn	Mo	Si	W	V	C
HT-9	0.5	12.0	0.2	1.0	0.25	0.5	0.5	0.2
AISI S-5	0.06	0.35	0.81	0.75	1.79	-	0.26	0.55
EP-823	0.8	12.0	0.6	1.0	1.3	0.8	0.4	0.2

Table 2. Composition (ppm) of Pb-Bi samples from the Control, hot leg (Hot) and the cold leg (Cold). Pb and Bi concentrations are in weight percent. Estimated accuracy is ± 10%.

	Cd	Cu	Fe	Ni	Sn	Zn	Si	Bi wt%	Pb wt%
Control	42.5	8.71	52.0	16.1	3280	31.6	247	49.5	49.3
Hot	42.5	16.8	32.7	10.5	3416	35.2	300	50.0	48.9
Cold	41.5	14.6	30.8	12.2	3414	29.6	259	50.4	46.9

Table 3. Comparison of oxygen partial pressures in equilibrium with various oxides at 550°C.

Oxide	Oxygen pressure (atm.)
Bi_2O_3	2.4×10^{-15}
PbO	4.3×10^{-18}
Fe_3O_4	1.6×10^{-27}
$FeCr_2O_4$	3.8×10^{-38}
Cr_2O_3	1.1×10^{-39}
SiO_2	4.9×10^{-49}

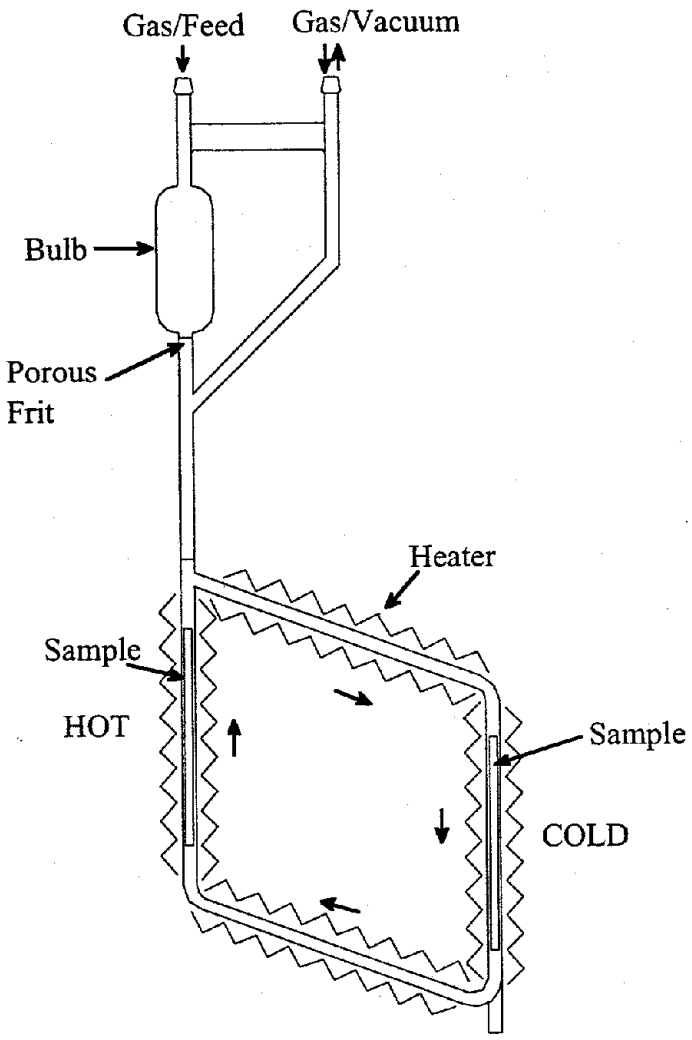

Fig. 1. Schematic drawing of a quartz convection harp installed in a furnace assembly

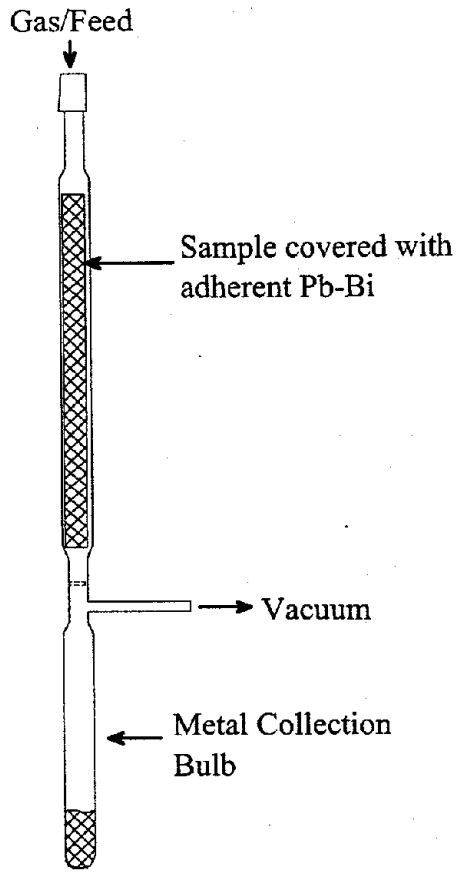

Fig. 2. Schematic drawing of filter tube

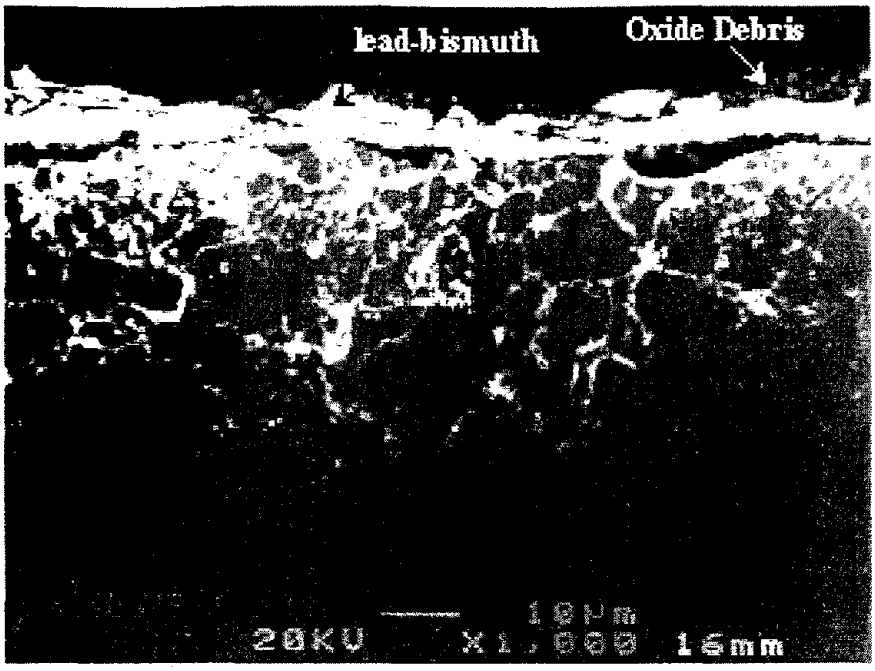

Fig. 3a. Micrograph of an AISI S-5 sample exposed to molten lead-bismuth in the hot leg of the convection harp. Penetration of the lead-bismuth into the sample (marked by arrows) is evident.

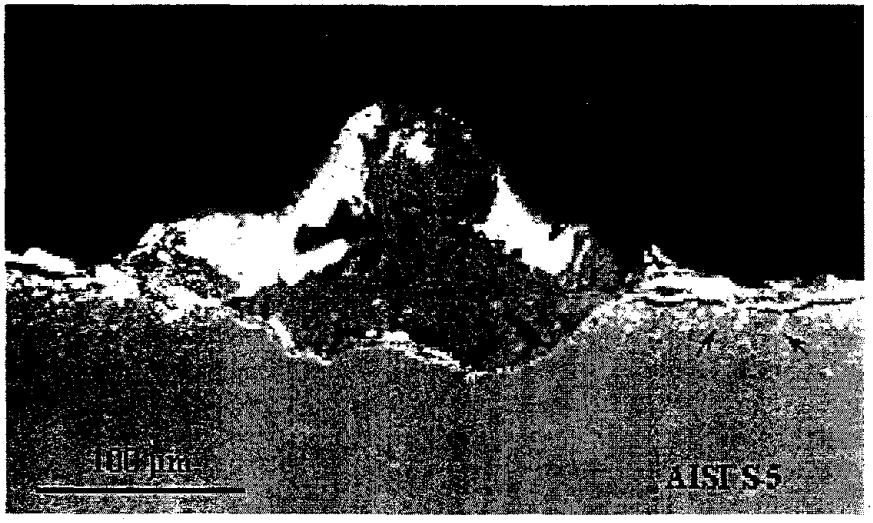

Fig. 3b. Same sample as in Fig. 3a, but showing the "debris" left behind by the attack. The arrows in the metal show the intergranular penetration

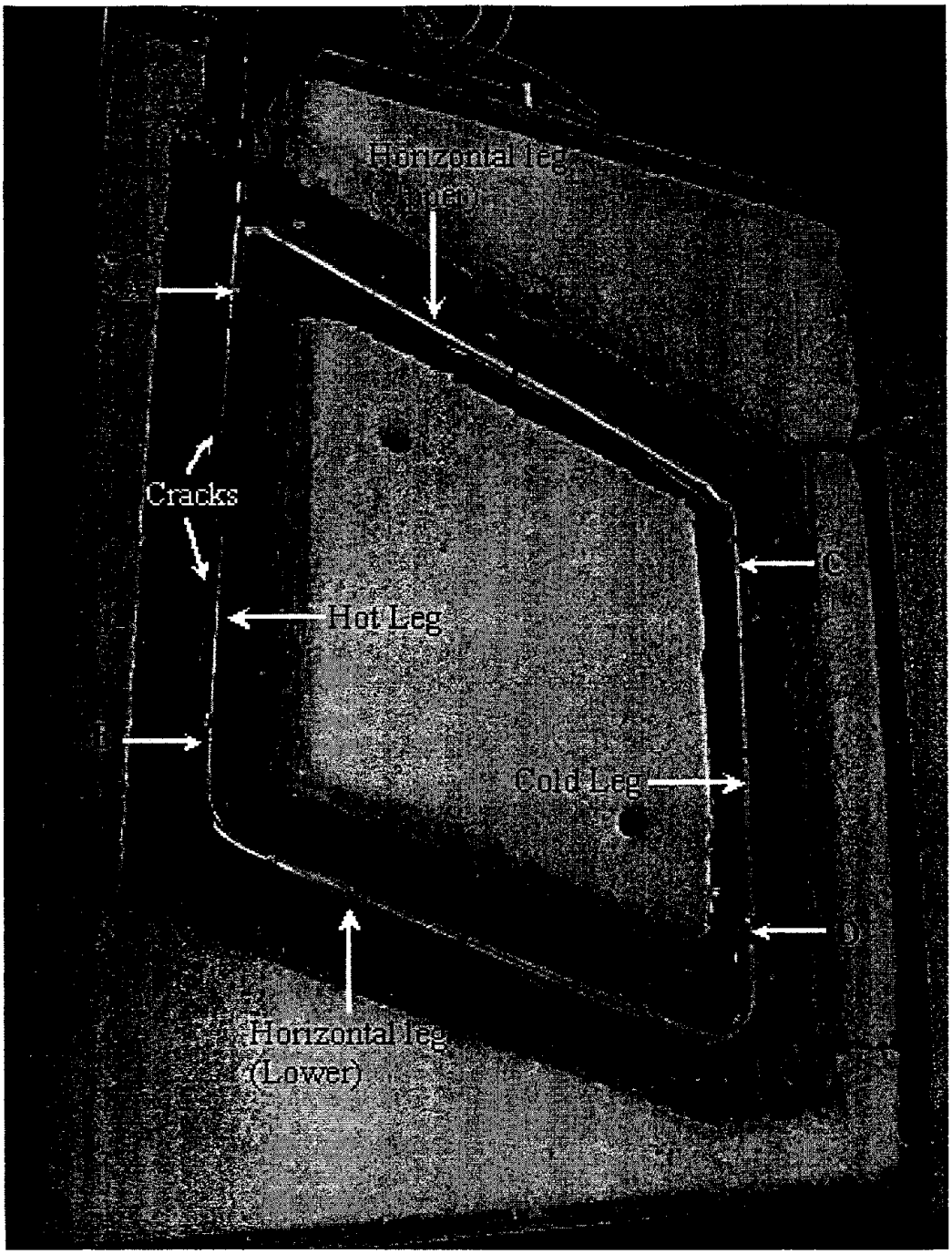

Fig. 4. Quartz convection harp after termination of the test showing sample locations. The quartz cracked after the assembly was cooled to room temperature.

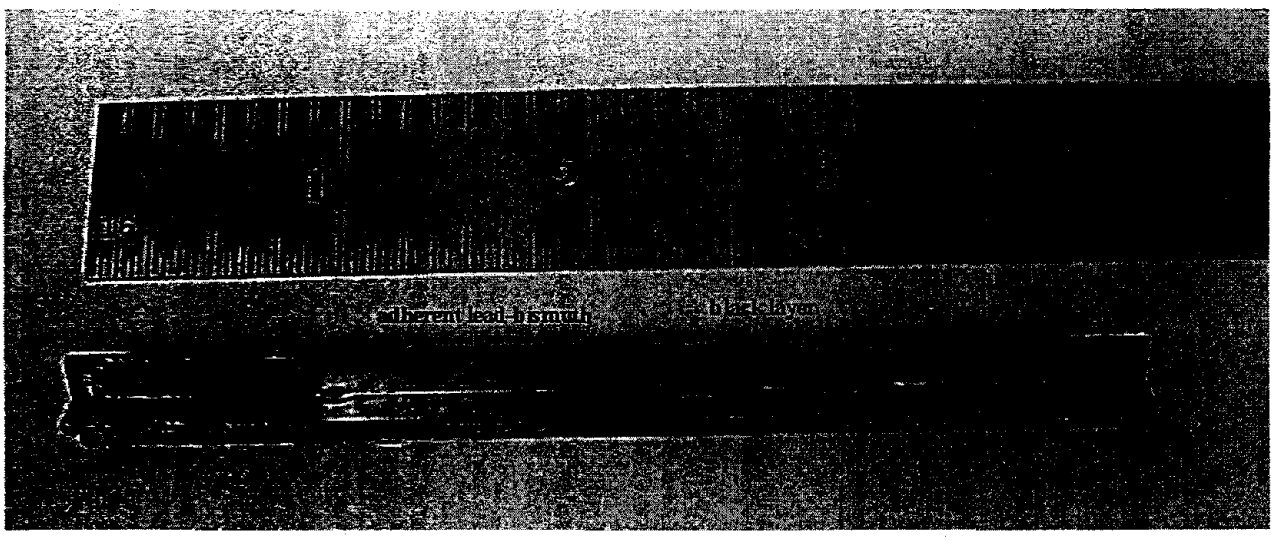

Fig. 5. HT-9 sample from hot leg (~550°C) of convection harp. Note the black layer under the adherent lead-bismuth.

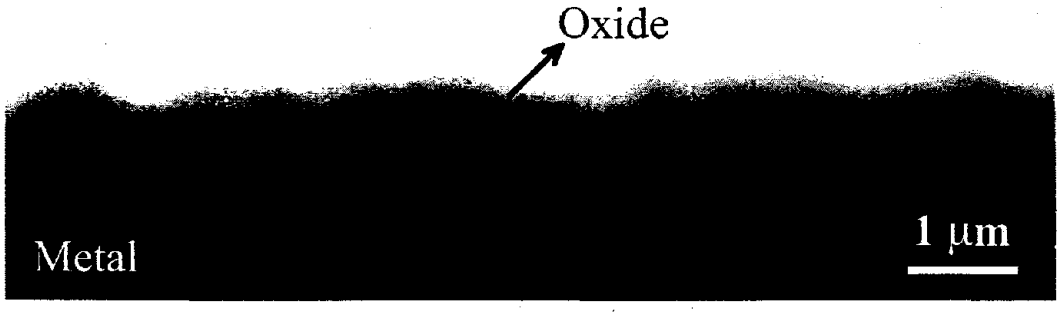

Fig. 6 SEM image of HT-9 after exposure to Pb-Bi. at ~550°C. Note thin surface layer.

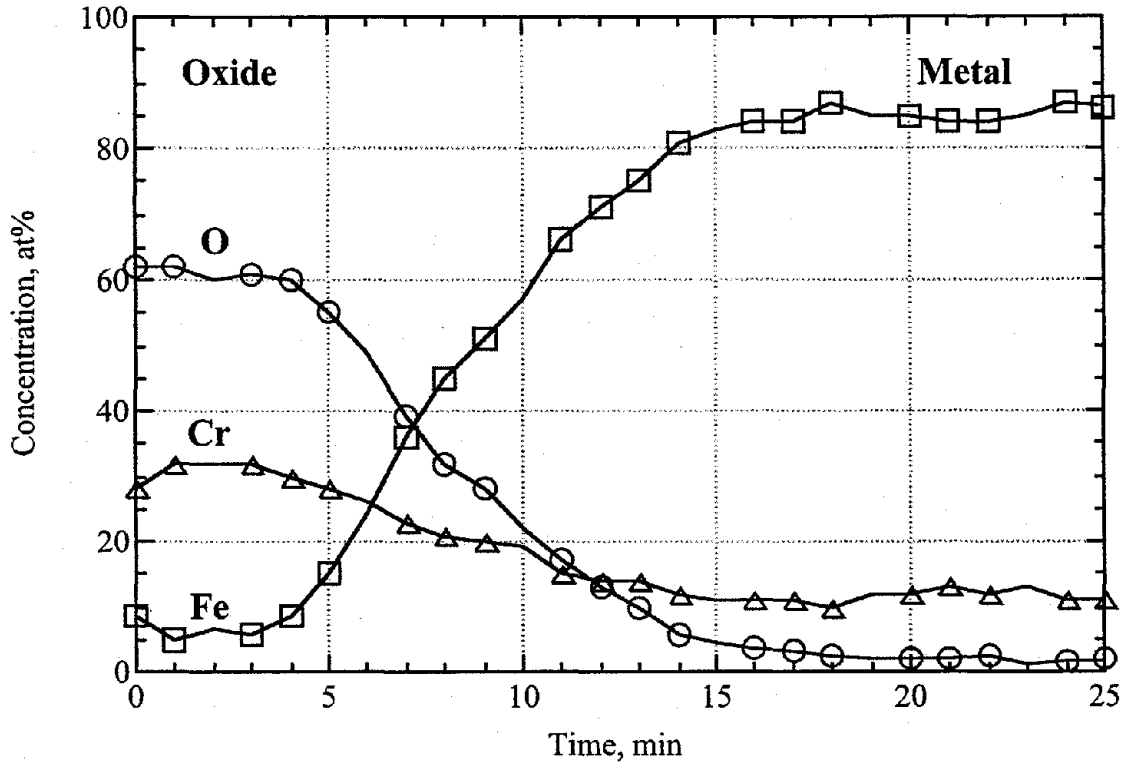

Fig. 7. Representative AES depth profile from HT-9 samples exposed to ~550°C lead-bismuth